nature energy

ARTICLES

https://doi.org/10.1038/s41560-018-0198-9

An intermediate temperature garnet-type solid electrolyte-based molten lithium battery for grid energy storage

Yang Jin[1,2,5], Kai Liu[1,5], Jialiang Lang[1], Denys Zhuo[3], Zeya Huang[1], Chang-an Wang[1], Hui Wu[1]* and Yi Cui[3,4]*

Batteries are an attractive grid energy storage technology, but a reliable battery system with the functionalities required for a grid such as high power capability, high safety and low cost remains elusive. Here, we report a solid electrolyte-based molten lithium battery constructed with a molten lithium anode, a molten Sn–Pb or Bi–Pb alloy cathode and a garnet-type $Li_{6.4}La_3Zr_{1.4}Ta_{0.6}O_{12}$ (LLZTO) solid electrolyte tube. We show that the assembled Li||LLZTO||Sn–Pb and Li||LLZTO||Bi–Pb cells can stably cycle at an intermediate temperature of 240 °C for about one month at current densities of 50 mA cm^{-2} and 100 mA cm^{-2} respectively, with almost no capacity decay and an average Coulombic efficiency of 99.98%. Furthermore, the cells demonstrate high power capability with current densities up to 300 mA cm^{-2} (90 mW cm^{-2}) for Li||LLZTO||Sn–Pb and 500 mA cm^{-2} (175 mW cm^{-2}) for Li||LLZTO||Bi–Pb. Our design offers prospects for grid energy storage with intermediate temperature operations, high safety margin and low capital and maintenance costs.

Smart grids require highly reliable and low-cost rechargeable batteries to integrate renewable energy sources as a stable and flexible power supply and to facilitate distributed energy storage[1–6]. As a promising technology for stationary energy storage, liquid metal electrode (LME) based batteries, which were invented in 1960s[7,8], possess excellent properties such as low cost, easy scale up, dendrite-free cycling, high power capability and long lifespan[9–12]. Lithium represents the best anode choice for LME batteries, as it is the lightest metal and has the lowest electrode potential (−3.04 V versus standard hydrogen potential) among all elements[13–15]. Previously reported LME batteries with molten lithium anodes primarily use molten liquid lithium salts as the electrolyte, which inevitably requires a high operating temperature (450 °C in an optimized case) due to the high melting point of lithium salts, making it difficult to maintain hermetic sealing of the batteries as well as resulting in high maintenance costs, serious corrosion and safety issues[16,17]. On the other hand, the dissolution of lithium in the molten salts leads to non-negligible self-discharge and relatively low Coulombic efficiency (<98%)[18]. By contrast, lithium ion solid electrolytes, which are considered as key materials for future lithium metal batteries and have been widely researched, can provide a high level of safety and reliability in physically and electronically separating the lithium anode from the cathode with no self-discharge and no lithium penetration or solubility[19–21]. Garnet-type solid electrolytes in particular have attracted increasing attention as promising candidates due to their high lithium ion conductivity, stability with lithium metal and wide electrochemical window[22–24]. Extensive efforts have been made to employ garnet electrolytes in lithium batteries for practical use, at room temperature[25–27]. However, there has been little success, and the major challenges are: the ionic conductivity of garnet electrolytes is still relatively low at room temperature (typically <1 mS cm^{-1}); the interfacial resistance between a garnet electrolyte and electrodes that are typically solid at room temperature is generally high. The low ionic conductivity and the high interfacial resistance result in a high internal resistance and consequently a poor power capability of the batteries, thus plaguing efforts to develop garnet, and many other types of solid electrolyte, for wide practical applications.

Instead of tackling the challenges within the limitation of room temperature, we note that the ionic conductivity of garnet solid electrolytes increases to a competitive level at elevated temperatures (>60 mS cm^{-1} above 200 °C based on our experimental data). Moreover, when a solid electrolyte is used in a system operating above the lithium melting point (180 °C), such as LME batteries, a liquid–solid interface is created instead of a solid–solid interface. As a result, the interfacial impedance can be largely decreased. Therefore, we believe that introducing garnet solid electrolyte to LME batteries with lithium anode may solve the problems related to the molten lithium salt electrolyte, and also open up a different direction for the development of lithium ion conductive solid electrolytes towards practical applications.

Here, based on a home-made garnet-type $Li_{6.4}La_3Zr_{1.4}Ta_{0.6}O_{12}$ (LLZTO) solid electrolyte tube, we design and assemble an LME battery with a molten lithium anode, and we select low-melting-point Sn–Pb and Bi–Pb alloy cathodes as two examples to test the battery performance. The LLZTO ceramic tube was employed for conduction of lithium ions and maintaining separation between the liquid metal electrodes. The battery demonstrates high current density (up to 500 mA cm^{-2}) and high efficiency (99.98% Coulombic efficiency and >75% energy efficiency) while operating at an intermediate temperature of 240 °C. These results lay a foundation for

[1]State Key Lab of New Ceramics and Fine Processing, School of Materials Science and Engineering, Tsinghua University, Beijing, China. [2]Department of Electrical Engineering, Zhengzhou University, Zhengzhou, China. [3]Department of Materials Science and Engineering, Stanford University, Stanford, CA, USA. [4]Stanford Institute for Materials and Energy Sciences, SLAC National Accelerator Laboratory, Menlo Park, CA, USA. [5]These authors contributed equally: Yang Jin, Kai Liu. *e-mail: huiwu@tsinghua.edu.cn; yicui@stanford.edu

the development of garnet solid-electrolyte-based molten lithium batteries in the grid energy storage field.

Configuration of Li||LLZTO||Alloy cells

The battery configuration schematic is shown in Fig. 1. A lithium metal anode is inside the LLZTO tube and a stainless steel rod is inserted serving as a current collector for the anode. An alloy cathode is in the stainless steel cylinder outside the LLZTO tube, separated from the lithium anode by the tube, and the cylinder is the current collector for the cathode at the same time. In this work, LLZTO tube electrolytes were fabricated using an appropriate doping strategy and an optimized ceramic sintering process (Supplementary Fig. 1). A Sn–Pb alloy (Sn:Pb = 75:25 mol%) and a Bi–Pb alloy (Bi:Pb = 75:25 mol%) were selected as the cathode materials due to their high lithiation plateaus (~0.7 V, Supplementary Fig. 2) and low melting points (183 °C for the Sn–Pb alloy and 197 °C for the Bi–Pb alloy). The addition of Pb decreases the melting point of the metal cathodes, and for the Sn–Pb cathode Pb also helps improve cyclability in the cell (Supplementary Figs. 3 and 4). The Li||LLZTO||Sn–Pb and Li||LLZTO||Bi–Pb batteries were tested at a temperature of 240 °C, which is above the melting point of both electrodes (Li metal and the alloys). At such a temperature, the molten lithium has good contact with the LLZTO tube: the interfacial resistance was found to be smaller than 0.4 Ω cm^2 based on a test of a Li||LLZTO||Li symmetrical cell (Supplementary Fig. 5). Silicone rubber, which is low cost and chemically and mechanically stable up to 250 °C, was used as a sealant and electrical insulator. A reliable seal and electrical insulation between electrodes are important to ensure safety and durability of an LME battery, and they will trigger an expensive manufacturing process if the operating temperature of the LME battery is too high, such as 300–350 °C in a Na–S battery[28]. Therefore, it will be highly beneficial for reducing the manufacturing cost to lower the operating temperature and enable conventional polymer sealing and electrical insulation technologies in an LME battery. Recently, great improvement has been achieved in another type of molten sodium-based battery, the ZEBRA battery, in terms of polymer sealing and insulation[29,30]. Here we verify that low-cost silicone rubber has good stability (Supplementary Figs. 6–8), and can be used in our LLZTO-tube-based molten lithium battery operating at 240 °C. The electrochemical results, which will be discussed later, confirm that the LLZTO tube electrolyte functions very well in the battery at this temperature.

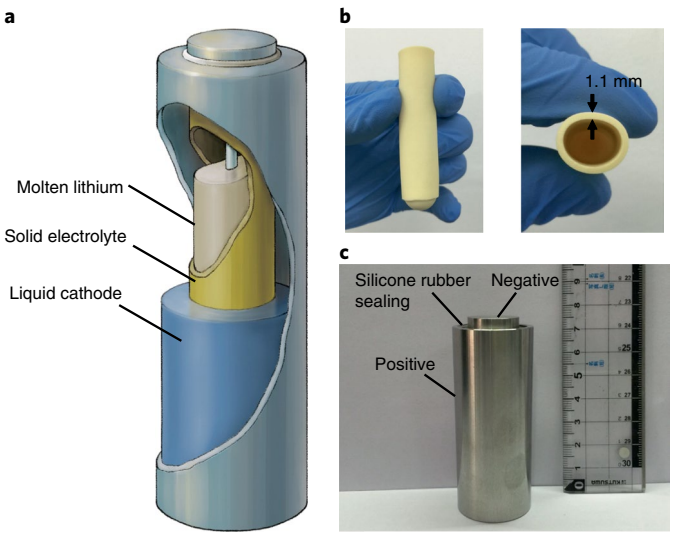

Fig. 1 | Schematic and optical image of the Li||LLZTO||liquid cathode battery. a, Schematic of the Li||solid electrolyte||liquid cathode battery. **b**, Digital photo of a U-shaped LLZTO tube. **c**, Digital photo of an assembled Li||LLZTO||Sn–Pb alloy battery.

Characteristics of the LLZTO solid electrolyte tube

Electrochemical impedance spectroscopy (EIS) measurements taken at different temperatures (Supplementary Figs. 9 and 10) show that the ionic conductivity of an LLZTO pellet (with the same formula as the LLZTO tube) can reach 85 mS cm^{-1} at 240 °C, which is ~240 times higher than its room temperature ionic conductivity (0.35 mS cm^{-1}), and is higher even than the ionic conductivity of organic liquid electrolytes at room temperature (~10 mS cm^{-1}, 1 mol $LiPF_6$ salt in 1:1 ethylene carbonate:ethyl methyl carbonate electrolyte at 30 °C)[31]. The relative density of the LLZTO tube is as high as 99% as measured by the Archimedes method with ethanol. Scanning electron microscopy (SEM) images taken from both the surface and cross-section of the tube (Supplementary Fig. 11), as well as the impermeability test result (Supplementary Fig. 12), also confirm the dense structure of the tube. Such a high relative density enables the LLZTO tube to prevent any leakage or crossover of the liquid metal electrodes, thereby ensuring the safety and reliability of the battery and a negligible self-discharge rate. Sufficient mechanical strength is also required in the LLZTO tube to withstand possible mechanical shock during cell assembling and operation. To verify its mechanical properties, we conduct a simulative shocking experiment using a shocking machine (Supplementary Video 1). From the recording video, it can be seen that even in a violent vibration and impact condition, the LLZTO tube still maintains intact without any noticeable crack or damage, indicating the tube has a good mechanical property. It is important to note that in our current lab-scale process, a 500 ml ball-milling container can prepare 100 g of LLZTO precursor at one time, which can produce a total of eight LLZTO tubes (12 g per tube) with 60 mm height and 12 mm diameter after sintering. These tubes show high uniformity in terms of morphology, density, colour and conductivity (Supplementary Fig. 13).

For grid energy storage applications, long service lifetime is a critical factor, which imposes a strict requirement that the LLZTO tube in our solid-electrolyte-based molten lithium battery must be stable for an extended period of time at an elevated temperature, especially against the highly reactive and corrosive molten lithium. We have characterized an LLZTO tube that has been immersed in molten lithium at 300 °C for 2 months. We found no lithium penetration, morphology change or phase change, demonstrating the excellent chemical and mechanical stability of the ceramic tubes at high temperatures (Supplementary Figs. 14–17)[32,33].

Performance of the Li||LLZTO||Sn–Pb cell

To test the battery design, first, a Li||LLZTO||Sn–Pb cell was assembled and cycled at a high current density of 50 mA cm^{-2} for a month (120 cycles) (Fig. 2). The voltage profiles in Fig. 2a,b show that the discharge and charge plateaus are ~0.6 V and ~0.8 V, respectively. Figure 2c demonstrates that as the cell is cycled, the cell has a stable volumetric capacity of ~254 mAh cm^{-3}, which is in accordance with its theoretical capacity corresponding to a discharge product with a molar ratio of Li:Sn:Pb = 3:15:5 (Supplementary Fig. 2). The capacity decay was very small during the whole process. The initial-cycle Coulombic efficiency is 93% which increases to 99.9% in the second cycle and stabilizes above 99.9% during the following long-term cycling. The average Coulombic efficiency is 99.98% (much higher than that of cells using molten salt electrolytes, which is about 98%)[16], which indicates that reaction of the electrode with the LLZTO tube or crossover through the LLZTO tube is negligible. The energy efficiency is stable at 75%. These results confirm the feasibility and reliability of this battery design, and further prove the stability of the LLZTO tube.

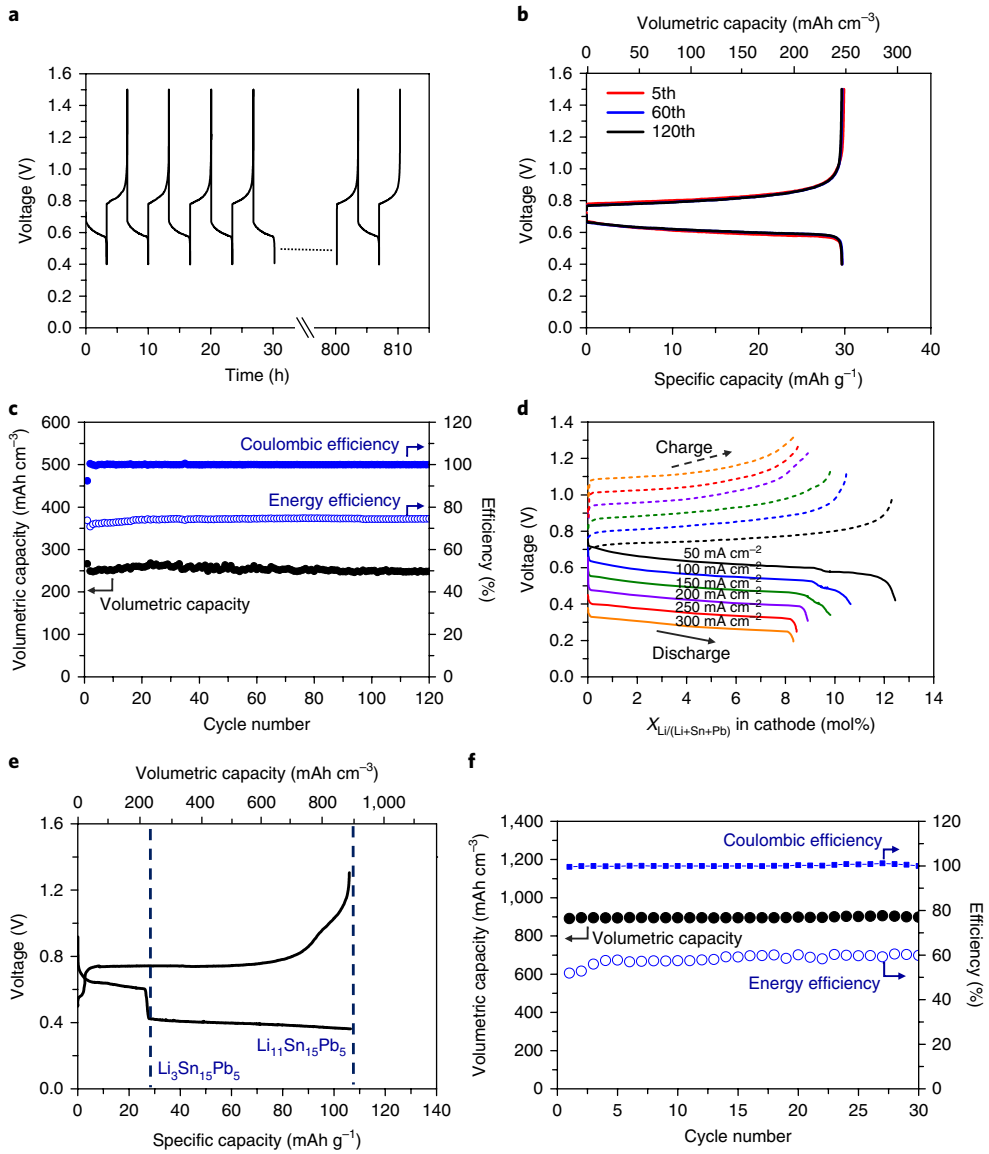

Fig. 2 | Electrochemical performance of a Li||LLZTO||Sn–Pb cell operating at 240 °C. a, Voltage profiles from 1 to 5 cycles and 119 to 120 cycles at 50 mA cm^{-2}. **b**, Representative voltage profiles during the 5th, 60th and 120th cycles. **c**, Coulombic efficiency, energy efficiency and volumetric capacity as a function of cycle number. In this experiment 3.561 g Sn and 2.073 g Pb were used as the cathode materials. **d**, Voltage profiles at different current densities (50–300 mA cm^{-2}). In this experiment 1.187 g Sn and 0.691 g Pb were used as the cathode material. When discharged to the first voltage jump, the elements molar ratio of the discharge product is Li:Sn:Pb = 3:15:5. **e**, Voltage profiles (5th cycle) of a constant capacity cycling Li||LLZTO||Sn–Pb cell at 50 mA cm^{-2}. The discharge capacity is set at 600 mAh and the charge cut-off voltage is set at 1.3 V. Two blue vertical dashed lines represent the points where the Sn–Pb alloy was lithiated to $Li_3Sn_{15}Pb_5$ and $Li_{11}Sn_{15}Pb_5$. **f**, Coulombic efficiency, energy efficiency and volumetric capacity as a function of cycle number of the constant capacity cycling Li||LLZTO||Sn–Pb cell in **e**. In this experiment 3.561 g Sn and 2.073 g Pb was used as the cathode materials. Specific and volumetric capacities were calculated based on the weight and volume of the Sn_3Pb alloy cathode, respectively.

Grid energy storage requires high power capability to facilitate incorporation of renewable energy when available and to respond quickly to shifts in demand on the grid to regulate peak loads. In our design, though based on a solid electrolyte, the LME battery still shows high power capability. The LLZTO tube electrolyte is able to function effectively in Li||LLZTO||Sn–Pb cells at 240 °C even at high current densities. Voltage profiles at different current densities ranging from 50–300 mA cm^{-2} are shown in Fig. 2d. For each current density increment of 50 mA cm^{-2}, the average discharge voltage showed a drop of only 70 mV. Even at a high current density of 300 mA cm^{-2}, the battery shows good cycle performance with a discharge voltage plateau of 0.3 V and achieving 62% of its theoretical capacity. The high power capability confirms the high ionic conductivity of the LLZTO solid electrolyte at 240 °C and the fast lithium ion charge transfer kinetics at the liquid electrode–solid electrolyte interfaces.

According to the coulometric titration result (Supplementary Fig. 2), the Li||LLZTO||Sn–Pb cell has a second plateau at ~0.47 V, during which Pb would participate in the discharge reaction as well (Supplementary Figs. 3 and 4). The second plateau ended till the elements ratio of the cathode reaches Li:Sn:Pb = 36:15:5. Therefore, after the first voltage jump, the cell can be further discharged to achieve a much higher cell capacity. As shown in Fig. 2e,f, by discharging the cell to its second plateau, a reversible volumetric capacity of 896 mAh cm^{-3} can be obtained, corresponding to a discharged cathode with elements mole ratio Li:Sn:Pb = 11:15:5.

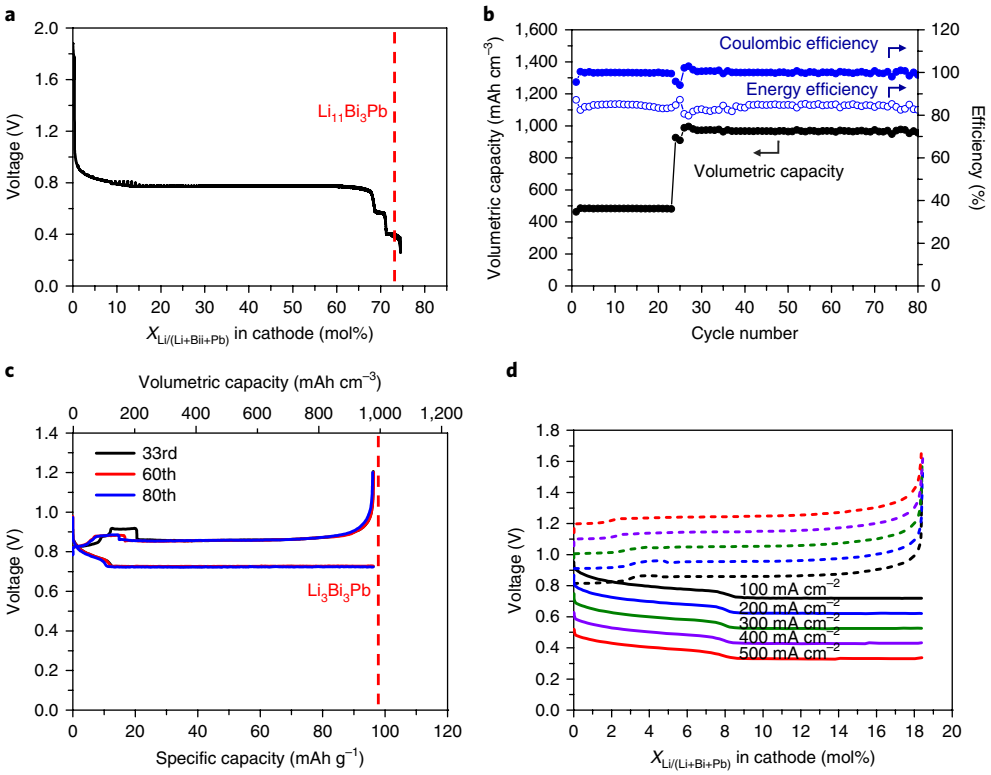

Fig. 3 | Electrochemical performance of a Li||LLZTO||Bi–Pb cell operating at 240 °C. a, Coulometric titration of a Li||LLZTO||Bi–Pb cell operating at 240 °C. The coulometric titration experiment was conducted by discharging the cell at a small current density of 5 mA cm^{-2} followed by a rest (zero current) of 10 min after every 5 mAh cm^{-2} increment of constant discharge capacity. A red vertical dashed line represents the point where the Bi–Pb alloy was lithiated to $Li_{11}Bi_3Pb$. **b**, Coulombic efficiency, energy efficiency and volumetric capacity as a function of cycle number at 100 mA cm^{-2}. The discharge capacity is set as 192 mAh (corresponding to a discharge product of $Li_{1.5}Bi_3Pb$) in the first 23 cycles and 384 mAh (corresponding to a discharge product of Li_3Bi_3Pb) in the following cycles. The charge cut-off voltage is set as 1.2 V. **c**, Representative voltage profiles. A red vertical dashed line represents the point where the Bi–Pb alloy was lithiated to Li_3Bi_3Pb. **d**, Voltage profiles at different current densities (100–500 mA cm^{-2}). In this experiment 3.000 g Bi and 0.991 g Pb were used as the cathode material. Specific and volumetric capacities were calculated based on weight and volume of the Bi_3Pb alloy cathode, respectively.

The cell's ability of deep discharge enables us, when necessary during practical use, to increase the accessible capacity of the battery at the price of decreased cell voltage by discharging the battery to the second plateau.

Safety is one of the major concerns over batteries used in grid energy storage. Conventional Na–S batteries face safety issues. If the beta-alumina tube broke, the molten Na and molten S would react seriously, and release a great deal of heat that could cause melting of the battery case and lead to fire and explosion. To test the safety of our LLZTO tube, we conduct a puncturing experiment using our Li||LLZTO||Sn–Pb cell. The process is shown in Supplementary Fig. 18. The LLZTO tube was full of molten Sn–Pb alloy (total 15 g), and the stainless steel case was full of molten lithium (about 2 g). The whole cell was heated in a box furnace at 300 °C and then moved out. The lithium metal and Sn–Pb alloy was in a totally liquid state. An infrared thermometer was used to detect the surface temperature of the cell. As shown, when moved out of the 300 °C box furnace, the surface temperature of the cell was detected to be 143.4 °C. Then we used a hammer to break the LLZTO tube, and the molten lithium and molten Sn–Pb alloy were mixed together. During the puncturing process, no smoking, sparking nor explosion happened. After puncturing, the surface temperature was detected to be 212.8 °C. The surface temperature increment was about 80 °C, and the stainless steel battery case remained intact without any melting or dissolution observed. These results show that our battery has a high safety margin.

Performance of the Li||LLZTO||Bi–Pb cell

Besides the Sn–Pb alloy, a Bi–Pb alloy can also be used as the cathode in our battery configuration, and an even better performance was measured. Figure 3a shows the coulometric titration of a Li||LLZTO||Bi–Pb cell operating at 240 °C. The cell was discharged at a small current density of 5 mA cm^{-2} followed by a rest (zero current) of 10 min after every 5 mAh cm^{-2} increment of constant discharge capacity. As can be seen, there are three voltage plateaus during the discharge: 0.77 V, 0.58 V and 0.40 V, with discharge capacities of 273, 29 and 67 mAh g^{-1} (based on the weight of Bi_3Pb), respectively. At the end of the voltage plateaus, the elemental molar ratio of Li:Bi:Pb in the cathode reached about 8.5:3:1, 9.4:3:1 and 11.5:3:1, respectively.

The difference between the voltages during rest and discharge reflect the internal resistance of the cell. As shown in Supplementary Fig. 19, as the discharge process went deeper, the voltage difference became larger, that is from ~5 mV at the first plateau to ~10 mV at the second one and ~18 mV at the third one, indicating the internal resistance of the cell increased. According to the Li–Bi phase diagram[34] and electrochemical performance of the Li||Bi cell[13] and the Li||Pb cell[14], we assume that the first plateau corresponds to Li–Bi alloying reaction resulting in solid state LiBi and Li_3Bi, whereas the following two lower plateaus could be attributed to alloying reactions that Pb participates in and has Li–Bi–Pb or Li–Pb alloy results that are also solid. As resultant solids accumulated and the liquid content decreased, the cathode–electrolyte interface changed

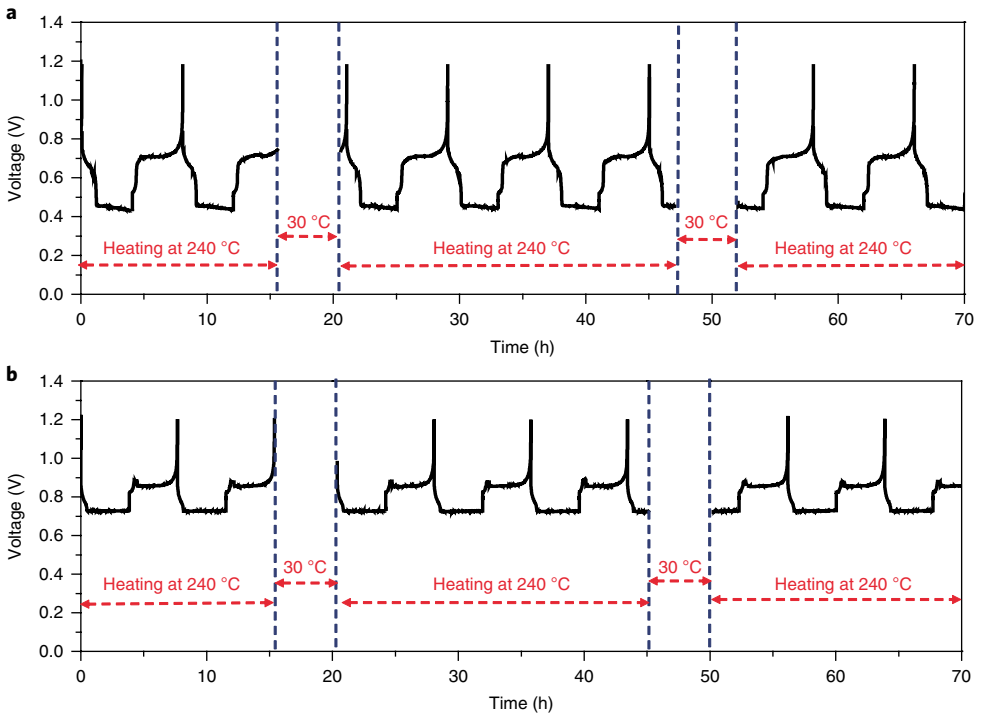

Fig. 4 | Freezing and thawing test of the Li||LLZTO||Sn–Pb cell and the Li||LLZTO||Bi–Pb cell. a, Li||LLZTO||Sn–Pb cell heating off for 5 h (drop to 30 °C) during charging and discharging process then back to 240 °C again. Current density: 50 mA cm^{-2}. In this experiment 1.567 g Sn and 0.911 g Pb were used as the cathode material. **b**, Li||LLZTO||Bi–Pb cell heating off for 5 h (drop to 30 °C) after fully charged and during discharging process then back to 240 °C again. Current density: 100 mA cm^{-2}. In this experiment 3.000 g Bi and 0.991 g Pb were used as the cathode material.

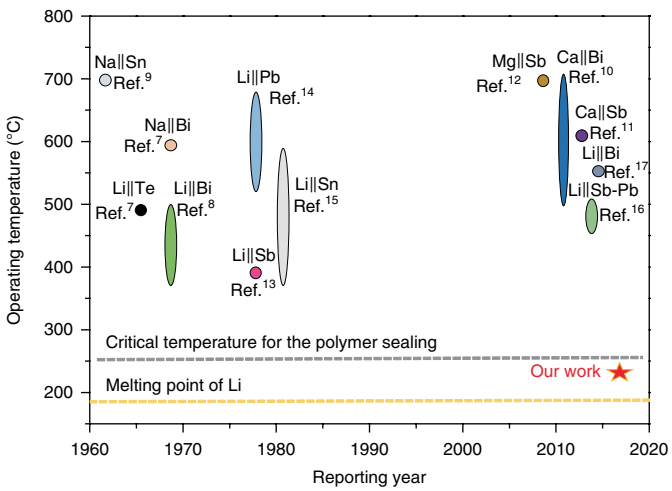

Fig. 5 | Operating temperature comparison of different LME batteries reported since 1960s.

from a liquid–solid to a solid–solid state, which could be the main reason for the increase of internal resistance. Figure 3b,c shows the electrochemical result of the assembled Li||LLZTO||Bi–Pb battery at 240 °C operation temperature with a current density of 100 mA cm^{-2}. When testing at this high current density, to avoid battery failure caused by the deterioration of the cathode–electrolyte interface and increase of irreversible capacity related to solid discharge products, we conducted constant capacity discharge during cycling tests to control the solid content in the cathode (in commercial Na–S batteries, generation of the solid discharge product is also controlled). The discharge capacity was set as 192 mAh (corresponding to a discharge product of $Li_{1.5}Bi_3Pb$) in the first 23 cycles and 384 mAh (corresponding to a discharge product of Li_3Bi_3Pb) in the following cycles. The charge cut-off voltage was set as 1.2 V. The cell worked stably in the discharge–charge cycling test, which lasted for about one month. The average Coulombic efficiency was about 99.98% and the average energy efficiency was about 84.1%. Figure 3d shows voltage profiles at different current densities ranging from 100–500 mA cm^{-2}. For each current density increment of 100 mA cm^{-2}, the average discharge voltage showed a drop of only 90 mV. Even at a high current density of 500 mA cm^{-2}, the battery shows good cycle performance with a discharge voltage plateau of 0.35 V (175 mW cm^{-2}).

Freezing and thawing test

The ability of the cell to recover after being cooled down is also of great importance for practical use in grid energy storage. The freeze/thaw volume excursions of the metals, especially the cathode in either a charged or discharged state, may lead to mechanical failure of the ceramic electrolyte tube. To investigate the thermal cyclability, we conducted freezing and thawing tests of the Li||LLZTO||Sn–Pb cell and Li||LLZTO||Bi–Pb cell, and the result is shown in Fig. 4. As can be seen in Fig. 4a (Li||LLZTO||Sn–Pb cell) and Fig. 4b (Li||LLZTO||Bi–Pb cell), after freezing and thawing, in either the charging or discharging process, the cell worked normally with no open nor short circuit, and even no fluctuation in cycle curves, which means there was no mechanical or electrochemical failure of the LLZTO tube.

Conclusion

By using a high quality garnet-type LLZTO tube electrolyte, we decreased the operating temperature of a molten lithium based LME battery to 240 °C, while enabling the cell to achieve high Coulombic efficiency (average 99.98%) and high power capability (up to 175 mW cm^{-2}). The operating temperature of our Li||LLZTO||Sn–Pb cell and Li||LLZTO||Bi–Pb cell compares favourable with other molten lithium batteries reported since 1960s (Fig. 5). The reduced

working temperature slows the oxidation and corrosion rate of the battery materials (particularly of the battery packaging materials in an air atmosphere) and also reduces the cost of sealing and electrical insulation process as polymer materials can be used at temperatures below 250 °C. Therefore, capital and maintenance costs of our LME battery could be lower than its counterparts that have to work at higher temperatures. Thanks to the high density of the Sn–Pb and Bi–Pb alloy, the Li||LLZTO||Sn–Pb and Li||LLZTO||Bi–Pb cells show a theoretical volumetric energy density as high as 570 Wh l^{-1} and 940 Wh l^{-1}, respectively (Supplementary Table 1). In terms of cost, according to the raw material cost, the price of the LLZTO material is about US$0.037 g^{-1} (Supplementary Table 2), and the theoretical full metal electrode cost of the Li||Sn–Pb and Li||Bi–Pb cell is estimated to be US$160 kWh^{-1} and US$80 kWh^{-1}, respectively (Supplementary Table 3). As can be seen, our solid-electrolyte-based molten lithium battery has good applicability and feasibility, and the two examples, especially the Li||LLZTO||Bi–Pb cell, have a great potential for grid-scale application. We also propose that, by implementing a better cathode with larger capacity and higher voltage, the performance of the battery can be further improved. All in all, the low cost and high performance of this solid-electrolyte-based molten lithium battery makes it a promising candidate for grid energy storage applications.

Methods

Fabrication and characterization of garnet-type LLZTO tube. Li_2CO_3 (Sinopharm, 99.99%), La_2O_3 (Sinopharm, 99.99%, dried at 900 °C for 12 h), ZrO_2 (Aladdin, 99.99%) and Ta_2O_5 (Ourchem, 99.99%) powders were mixed together at a molar ratio of $Li_{6.4}La_3Zr_{1.4}Ta_{0.6}O_{12}$ (30% excess Li_2CO_3 was added) and ground with an agate mortar and pestle and then heated at 900 °C for 6 h to decompose the metal salts. The resulting powders were ball milled for 12 h, before being pressed into a U-shaped tube under 220 MPa cold isostatic pressing for 90 s, and then annealed at 1,140 °C for 16 h in air while the tubes were covered with the same mother powder. All heat treatments were conducted in alumina crucibles (>99% Al_2O_3) covered with alumina lids. The Archimedes water displacement method was used to measure the relative density of the LLZTO tube. XRD (Bruker AXS D8 Advanced with Da Vinci) was used to monitor phase formation. The tube's microstructure was examined using a field-emission SEM (Shimadzu SSX-550). A broadband dielectric spectrometer (NOVOCOOL) was used to carry out the impedance spectroscopy measurement (frequency range: 40 Hz to 10 MHz; a.c. voltage: 10 mV; temperature: 25–300 °C).

Assembly and electrochemical measurements. Sn and Pb particles (75:25 mol%) or Bi and Pb particles (75:25 mol%) were first put into a stainless steel cell and heated for 1 h at 400 °C in a box furnace (MTI) to form a Sn–Pb alloy with a melting point of 183 °C, and a Bi–Pb alloy with a melting point of 197 °C. Then, lithium metal was put into the garnet-type LLZTO tube and heated in a box furnace (MTI) at 240 °C for 20 min to melt the lithium metal. The LLZTO tube with molten lithium inside was then put into the molten Sn–Pb or Bi–Pb alloy at 240 °C. A 1 mm diameter stainless steel rod was inserted into the molten lithium as the anode current collector. After the cell cooled down to room temperature, silicone rubber was used to seal the cell with a stainless steel cap. The whole assembly process was conducted in an Argon atmosphere glove box. The electrochemical performance of the Li||LLZTO||Sn–Pb and Li||LLZTO||Bi–Pb cells were tested in an Argon filled box furnace (MTI) at 240 °C, using a battery test system (LAND 2001 CT battery tester). The active surface area of all the cells is 1 cm^2 determined by the contact area between the LLZTO tube and the molten lithium.

Freezing and thawing tests. As shown in Fig. 4, during the charging process of the Li||LLZTO||Sn–Pb cell (Li||LLZTO||Bi–Pb cell), the testing programme was suspended and the heating equipment shut down, and temperature of the cell dropped and levelled off at 30 °C. Heat-off status was maintained for 5 h. Then the heating equipment was turned on and the temperature increased to 240 °C, and the testing programme started again. When the Li||LLZTO||Sn–Pb cell (Li||LLZTO||Bi–Pb cell) was discharging, the heating equipment was shut down and the battery testing programme suspended. Heat-off status was maintained for 5 h, and during this period the temperature of the cell dropped to 30 °C. Then the heating equipment was turned on, the testing programme started again and the discharge process continued. The temperature went back to 240 °C and was kept at 240 °C.

Impermeability test of the LLZTO sheet. A previously reported test method was used[35]. An LLZTO cylinder with a diameter of 15 mm and a height of 5 mm was synthesized using the same process as synthesizing the LLZTO tube. Then a 200-μm-thick LLZTO sheet was obtained by cutting the LLZTO cylinder using a low-speed diamond saw. In the test, gas pressure difference on two sides of the LLZTO sheet was increased gradually until the sheet ruptured. Gas flow rate on the ambient air side and the maximum pressure difference the LLZTO sheet could stand were recorded. The result is shown in Supplementary Fig. 12, gas flow rate in the LLZTO sheet test remained zero until the sheet broke at a pressure difference of 134 kPa. This result verifies the impermeability of the electrolyte, which is directly related to the lithium anode protection and liquid lithium blocking ability of the electrolyte. As the sheet is very thin (200 μm), it's reasonable to believe that the 1.1 mm thick LLZTO tube also has a good impermeability against liquid metal.

Data availability. The data that support the plots within this paper and other findings of this study are available from the corresponding authors upon reasonable request.

Received: 24 June 2017; Accepted: 5 June 2018;
Published online: 02 July 2018

References

1. Chu, S. & Majumdar, A. Opportunities and challenges for a sustainable energy future. *Nature* **488**, 294–303 (2012).
2. Chu, S., Cui, Y. & Liu, N. The path towards sustainable energy. *Nat. Mater.* **16**, 16–22 (2017).
3. Armand, M. & Tarascon, J. M. Building better batteries. *Nature* **451**, 652–657 (2008).
4. Dunn, B., Kamath, H. & Tarascon, J. M. Electrical energy for the grid: a choice of battery. *Science* **334**, 928–935 (2011).
5. Li, L. Y. et al. A stable vanadium redox-flow battery with high energy density for large-scale energy storage. *Adv. Energy Mater.* **1**, 394–400 (2011).
6. Wang, W. et al. Recent progress in redox fow battery research and development. *Adv. Func. Mater.* **23**, 970–986 (2013).
7. Cairns, E. J. et al. *Galvanic Cells with Fused-Salt Electrolytes* Technical report ANL-7316 (Argonne National Laboratory, 1967).
8. Shimotake, H., Rogers, G. & Cairns, E. Secondary cells with lithium anodes and immobilized fused-salt electrolytes. *Ind. Eng. Chem. Proc. Des. Dev.* **8**, 51–56 (1969).
9. Weaver, R. D., Smith, S. W. & Willmann, N. L. The sodium|tin liquid-metal cell. *J. Electrochem. Soc.* **109**, 653–657 (1962).
10. Kim, H., Boysen, D. A., Ouchi, T. & Sadoway, D. R. Calciume-bismuth electrodes for large-scale energy storage (liquid metal batteries). *J. Power Sources* **241**, 239–248 (2013).
11. Ouchi, T., Kim, H., Ning, X. H. & Sadoway, D. R. Calcium-antimony alloys as electrodes for liquid metal batteries. *J. Electrochem. Soc.* **161**, A1898–A1904 (2014).
12. Bradwell, D. J., Kim, H., Sirk, A. H. & Sadoway, D. R. Magnesium-antimony liquid metal battery for stationary energy storage. *J. Am. Chem. Soc.* **134**, 1895–1897 (2012).
13. Weppner, W. & Huggins, R. Thermodynamic properties of the intermetallic systems lithium-antimony and lithium-bismuth. *J. Electrochem. Soc.* **125**, 71–4 (1978).
14. Saboungi, M. L., Marr, J. & Blander, M. Thermodynamic properties of a quasi-ionic alloy from electromotive force measurements: the Li-Pb system. *J. Chem. Phys.* **68**, 1375–1384 (1978).
15. Wen, C. J. & Huggins, R. A. Thermodynamic study of the lithium-tin system. *J. Electrochem. Soc.* **128**, 1181–1187 (1981).
16. Wang, K. L. et al. Lithium-antimony-lead liquid metal battery for grid-level energy storage. *Nature* **514**, 348–350 (2014).
17. Ning, X. H. et al. Self-healing Li-Bi liquid metal battery for grid-scale energy storage. *J. Power Sources* **275**, 370–376 (2015).
18. Li, H. et al. Liquid metal electrodes for energy storage batteries. *Adv. Energy Mater.* **6**, 1600483 (2016).
19. Lu, X. et al. Liquid-metal electrode to enable ultra-low temperature sodium–beta alumina batteries for renewable energy storage. *Nat. Commun.* **5**, 4578 (2014).
20. Thangadurai, V., Pinzaru, D., Narayanan, S. & Baral, A. K. Fast solid-state Li ion conducting garnet-type structure metal oxides for energy storage. *J. Phys. Chem. Lett.* **6**, 292–299 (2015).
21. Liu, K. & Wang, C. A. Garnet-type $Li_{6.4}La_3Zr_{1.4}Ta_{0.6}O_{12}$ thin sheet: fabrication and application. *Electrochem. Commun.* **48**, 147–150 (2014).
22. Liu, K., Ma, J. T. & Wang, C. A. Excess lithium salt functions more than compensating for lithium loss when synthesizing $Li_{6.5}La_3Ta_{0.5}Zr_{1.5}O_{12}$ in alumina crucible. *J. Power Sources* **260**, 109–144 (2014).
23. Thangadurai, V., Kaack, H. & Weppner, W. J. F. Novel fast lithium ion conduction in garnet-type $Li_5La_3M_2O_{12}$ (M = Nb, Ta). *Cheminform* **34**, 437–440 (2003).
24. O'Callaghan, M. P., Powell, A. S., Titman, J. J., Chen, G. Z. & Cussen, E. J. Switching on fast lithium ion conductivity in garnets: the structure and transport properties of $Li_{3-x}Nd_3Te_{2-x}Sb_xO_{12}$. *Chem. Mater.* **20**, 2360–2369 (2008).

25. Han, X. et al. Negating interfacial impedance in garnet-based solid-state Li metal batteries. *Nat. Mater.* **16**, 572–579 (2017).
26. Jalem, R. et al. Concerted migration mechanism in the Li ion dynamics of garnet-type $Li_7La_3Zr_2O_{12}$. *Chem. Mater.* **25**, 425–430 (2013).
27. Liu, Y. Y. et al. Transforming from planar to three-dimensional lithium with flowable interphase for solid lithium metal batteries. *Sci. Adv.* **3**, eaao0713 (2017).
28. Lu, X., Xia, G., Lemmon, J. P. & Yang, Z. Advanced materials for sodium-beta alumina batteries: Status, challenges and perspectives. *J. Power Sources* **195**, 2431–2442 (2010).
29. Li, G. et al. Advanced intermediate temperature sodium–nickel chloride batteries with ultra-high energy density. *Nat. Commun.* **7**, 10683 (2016).
30. Chang, H. J. et al. Development of intermediate temperature sodium nickel chloride rechargeable batteries using conventional polymer sealing technologies. *J. Power Sources* **348**, 150–157 (2017).
31. Ding, M. S. et al. Change of conductivity with salt content, solvent composition, and temperature for electrolytes of $LiPF_6$ in ethylene carbonate-ethyl methyl carbonate. *J. Electrochem. Soc.* **148**, A1196–A1204 (2001).
32. Tietz, F. et al. Synthesis and Raman micro-spectroscopy investigation of $Li_7La_3Zr_2O_{12}$. *Solid State Ion.* **230**, 77–82 (2013).
33. Jin, Y. & McGinn, P. J. Al-doped $Li_7La_3Zr_2O_{12}$ synthesized by a polymerized complex method. *J. Power Sources* **196**, 8683–8687 (2011).
34. Gasior, W., Moser, Z. & Zakulski, W. Bi-Li system thermodynamic properties and the phase diagram calculations. *Arch. Metall.* **39**, 355–369 (1994).
35. Liu, K. & Wang, C. A. Honeycomb-alumina supported garnet membrane: composite electrolyte with low resistance and high strength for lithium metal batteries. *J. Power Sources* **281**, 399–403 (2015).

Acknowledgements

Y.C. acknowledges support from the Joint Center for Energy Storage Research, a battery hub under the US Department of Energy. H.W. acknowledges support from the National Basic Research of China (Grants 2015CB932500), National Natural Science Foundations of China (grants 51661135025 and 51522207). C.A.W. acknowledges support from the National Natural Science Foundations of China (grant 51572145).

Author contributions

Y.J., K.L., H.W. and Y.C. conceived the idea. Y.J. and K.L. designed the battery cells and conducted the electrochemical measurements. J.L. and Z.H. conducted SEM and XRD characterization. H.W. and Y.C. supervised the project. Y.J., K.L. D.Z., C.A.W., H.W. and Y.C. contributed to writing the manuscript. Y.J. and K.L. contributed equally to this work. All authors discussed the results and commented on the manuscript.

Competing interests

The authors declare no competing interests.

Additional information

Supplementary information is available for this paper at https://doi.org/10.1038/s41560-018-0198-9.

Reprints and permissions information is available at www.nature.com/reprints.

Correspondence and requests for materials should be addressed to H.W. or Y.C.

Publisher's note: Springer Nature remains neutral with regard to jurisdictional claims in published maps and institutional affiliations.